

IEICE **TRANSACTIONS**

on Information and Systems

VOL. E104-D NO. 10
OCTOBER 2021

The usage of this PDF file must comply with the IEICE Provisions on Copyright.

The author(s) can distribute this PDF file for research and educational (nonprofit) purposes only.

Distribution by anyone other than the author(s) is prohibited.

A PUBLICATION OF THE INFORMATION AND SYSTEMS SOCIETY



The Institute of Electronics, Information and Communication Engineers
Kikai-Shinko-Kaikan Bldg., 5-8, Shibakoen 3 chome, Minato-ku, TOKYO, 105-0011 JAPAN

Per-Pixel Water Detection on Surfaces with Unknown Reflectance

Chao WANG^{†a)}, Student Member, Michihiko OKUYAMA[†], Nonmember, Ryo MATSUOKA^{††},
and Takahiro OKABE[†], Members

SUMMARY Water detection is important for machine vision applications such as visual inspection and robot motion planning. In this paper, we propose an approach to per-pixel water detection on unknown surfaces with a hyperspectral image. Our proposed method is based on the water spectral characteristics: water is transparent for visible light but translucent/opaque for near-infrared light and therefore the apparent near-infrared spectral reflectance of a surface is smaller than the original one when water is present on it. Specifically, we use a linear combination of a small number of basis vector to approximate the spectral reflectance and estimate the original near-infrared reflectance from the visible reflectance (which does not depend on the presence or absence of water) to detect water. We conducted a number of experiments using real images and show that our method, which estimates near-infrared spectral reflectance based on the visible spectral reflectance, has better performance than existing techniques.

key words: water detection, absorption, hyperspectral imaging, NIR, spectral reflectance

1. Introduction

Detecting water on object surfaces such as road surfaces, floors, and manufactured products is important for various applications such as autonomous driving systems, robot path planning [1], [2], and visual inspection [3], [4]. In spite of its importance, water detection has received little attention in computer vision literature.

Image-based water detection is a challenging problem. This is because water is transparent for visible wavelengths, and then the appearance of water on an object surface significantly depends not on water itself but on the background object surface. Therefore, it is difficult to distinguish surfaces with/without water from ordinary color images.

Interestingly, it is known that water is translucent or opaque for near infrared (NIR) wavelengths, because water absorbs NIR light [5]. Therefore, observing at NIR wavelengths, the brightness of an object surface on which water is present is smaller than that without water, because NIR light, incoming to and outgoing from the object surface, is absorbed by water. In other words, the *apparent* spectral reflectance, *i.e.* the ratio between the spectral radiance observed at a surface point and the spectral irradiance, is

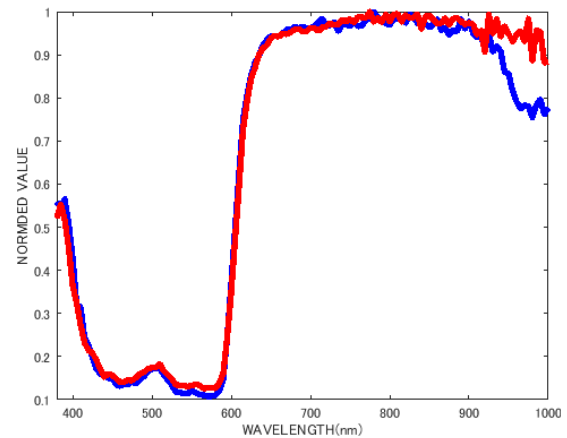


Fig. 1 The apparent spectral reflectance at a surface point when water is absent (red line) and present (blue line) in it.

smaller when water is present (see Fig. 1). Hence, we could detect water if the *original* spectral reflectance of an object surface without water is known, and if the apparent spectral reflectance of the point is smaller than the original one for NIR wavelengths.

However, the original spectral reflectances of object surfaces are unknown and spatially varying in general. Therefore, when the apparent spectral reflectance of an object surface is small, we cannot distinguish two cases: one is that the original spectral reflectance itself is small, and another is that the apparent spectral reflectance is small due to the absorption by water.

Accordingly, in this paper, we propose a method for per-pixel water detection via hyperspectral imaging. Specifically, our proposed method estimates the original spectral reflectance at each surface point in NIR wavelengths from its apparent spectral reflectance in visible wavelengths, that are invariant to the presence/absence of water. To this end, we make use of the low-dimensional linear combination model for spectral reflectance from visible to NIR wavelengths. Then, water is detected on the basis of the difference between the estimated original spectral reflectance and the apparent one in NIR wavelengths. To demonstrate the effectiveness of our method, we conducted a number of experiments using real images, and then showed that our method works better than existing methods.

The main contributions of this study are twofold. First, we propose a method for per-pixel water detection via hyperspectral imaging on the basis of wavelength-dependent

Manuscript received January 10, 2021.

Manuscript revised April 26, 2021.

Manuscript publicized June 6, 2021.

[†]The authors are with Department of Artificial Intelligence, Kyushu Institute of Technology, Iizuka-shi, 820–8502 Japan.

^{††}The author is with Faculty of Environmental Engineering, The University of Kitakyushu, Kitakyushu-shi, 808–0135 Japan.

a) E-mail: c.wang@pluto.ai.kyutech.ac.jp

DOI: 10.1587/transinf.2021PCP0002

opacity of water. Our method enables us to detect water on surfaces with unknown and spatially-varying reflectance. Second, we experimentally show that the spectral reflectances from visible to NIR wavelengths are approximately represented by using the low-dimensional linear combination model. The spectral reflectance estimated on the basis of the low-dimensional model would be useful for other applications such as spectral rendering and material classification.

2. Related Work

Water Detection: In remote sensing literature, there are well-known methods such as NDWI, HDWI, and their extension methods [6], [7]. These methods focus on detecting water bodies such as rivers, ponds, and oceans. On the other hand, we focus on detecting water on surfaces where the reflectance is unknown and spatially-varying. Therefore, the purpose of our method is different from these methods. In computer vision literature, in general, static water has sky reflection outdoors, and then the area of water with sky reflection can be easily distinguished from other terrain by brightness [8], [9]. However, outdoor water detection is still very challenging when sky reflection is not observed. If there is water on an object surface, the ratio of the spectral radiances on the surface at the two specific NIR bands will change greatly when the lighting is constant [10]. However, the spectral reflectance of surfaces such as factory automation is unknown and non-uniform, which makes it more difficult to identify water using only NIR spectral reflectances. Water is the most complicated case. Because the appearance of water on an object's surface significantly depends not on the water itself but on the background object surface. Despite this variability, water absorbs light, different colors of water and different backgrounds are classified by LDA [11]. However, it may be affected by the depth of the water to obtain undesired results. In contrast to the above methods, our method pays more attention to the property that water is transparent in visible wavelengths and translucent/opaque in the NIR wavelengths.

Hyperspectral Characteristics of Water: Shimano *et al.* [12], [13] proposed a method for wetness estimation on the basis of spectral analysis. Specifically, by analyzing the scattering of light inside the wet object, the change in the spectral brightness in the visible wavelengths due to water wetting is explained. Asano *et al.* [14] proposed a method of estimating the depth of objects in water on the basis of the multi-wavelength images using the fact that water absorbs NIR light. When light travels in water, water rarely absorbs visible light, which explains why water appears transparent to human eyes. In contrast, water absorbs NIR light from 830 nm to 1000 nm. In contrast to this approach, our method focuses not only on the visible spectral reflectance or the NIR spectral reflectance but on the connections between them.

Hyperspectral Object Detection: Hyperspectral imagery has been used in reconnaissance and surveillance ap-

plications where targets of interest are detected and identified [15]. The orthogonal subspace projection (OSP) algorithm [16] maximizes the signal-to-noise ratio (SNR) in the subspace orthogonal to the background subspace. However, this method requires background information beforehand, which is generally not achievable. The automatic target generation process (ATGP) [17] generates a set of targets from image data in an unsupervised manner which will subsequently be classified. It can be used to search for a specific target in unknown scenes. Compared with the classical detection technology, we propose a novel method for estimating NIR reflectance from visible reflectance, which solves the problem of detecting water and background when the background is complex and unknown. Chakrabarti and Zickler [18] use hyperspectral images of indoor and outdoor scenes, derive an optimized spatio-spectral basis for representing hyperspectral image patches using PCA, and explore statistical models for the coefficients in this basis. We proposed a method for estimating a NIR spectral reflectance from an apparent spectral reflectance in a visible light range on the basis of the spectral correlation between visible and NIR wavelengths.

3. Proposed Method

3.1 Outline

In this Section, we explain the details of our proposed method. First, we describe a low-dimensional linear model of spectral reflectance from visible to NIR wavelengths. Second, we explain how to estimate the original spectral reflectance in NIR wavelengths from the apparent spectral reflectance in visible wavelengths under the assumption that the spectral irradiance of a scene is known. Third, we describe per-pixel water detection on the basis of the difference between the apparent and estimated original spectral reflectances in NIR wavelengths. Figure 2 shows the flowchart of our method.

3.2 Low-Dimensional Linear Model

Parkkinen *et al.* [19] studied the spectral reflectances of the Munsell Color Book chips, and showed that the spectral reflectances in visible wavelengths are approximately represented by linear combinations of the basis functions derived via Principal Component Analysis (PCA). Specifically, a spectral reflectance $\rho(\lambda)$ is represented as

$$\rho(\lambda) \approx \sum_{n=1}^N c_n b_n(\lambda), \quad (1)$$

where λ stands for the wavelength of incoming and outgoing light, and $b_n(\lambda)$ and c_n are the n -th basis function ($n = 1, 2, 3, \dots, N$) and its coefficient respectively.

In contrast to Parkkinen *et al.*, we study the spectral reflectances of the Munsell Color Book chips not only in visible wavelengths but also in NIR wavelengths. We experimentally show that the low-dimensional linear model in

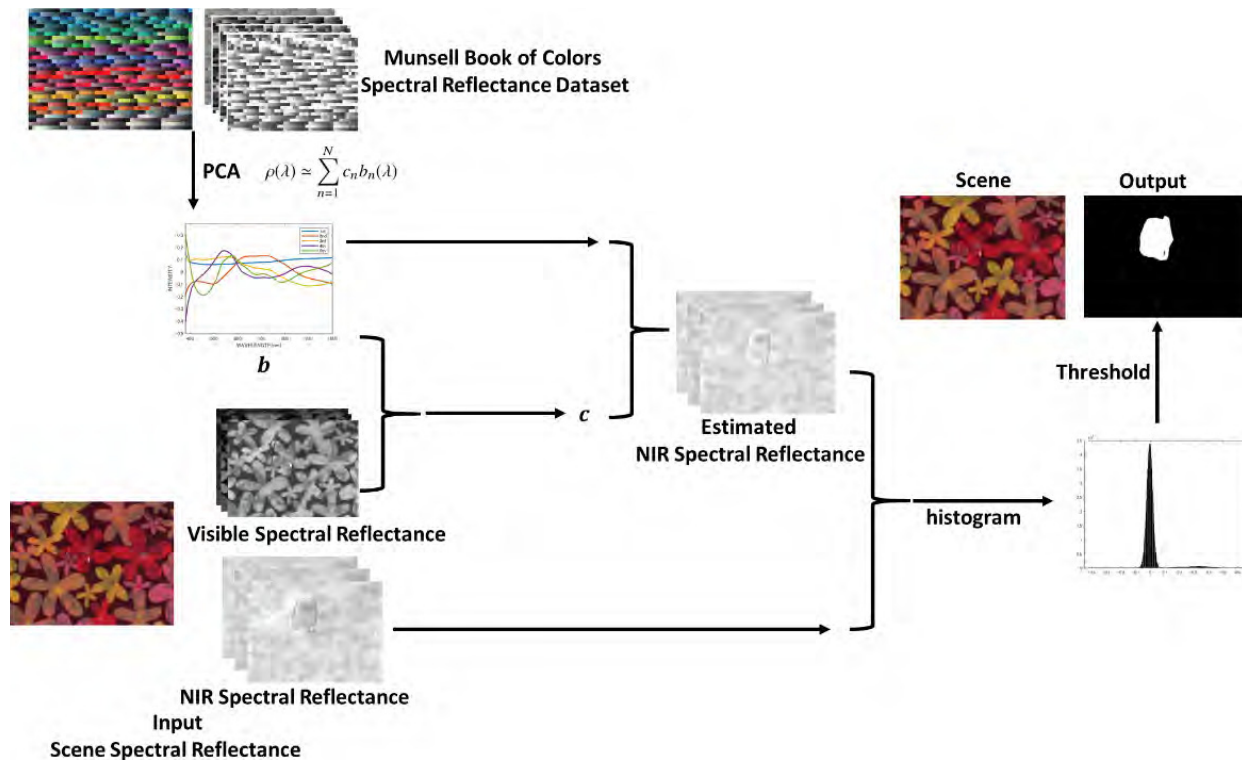


Fig. 2 The flowchart of our proposed method for per-pixel water detection.

Eq. (1) is applicable not only to visible wavelengths but also to visible to NIR wavelengths.

3.3 Estimation of NIR Spectral Reflectance

We capture an image of a scene of interest by using a hyperspectral camera. Suppose that the spectral irradiance of the scene is uniform and known up to per-pixel scale, i.e. the scene is illuminated by a single light source or multiple light sources with the same spectral intensity. The per-pixel spectral irradiance can be measured up to a scale by taking a hyperspectral image of the scene and the white balance and diffuse reflectance target of Spectralon at the same time for example.

We denote the spectral radiance and irradiance at a certain surface point by $s(\lambda)$ and $l(\lambda)$ respectively. Then, the apparent spectral reflectance $\hat{\rho}(\lambda)$ at the surface point is given by[†]

$$\hat{\rho}(\lambda) = \frac{s(\lambda)}{l(\lambda)}. \quad (2)$$

We assume that surfaces of interest are opaque and water-repellent, and that water is clear, containing no scattering medium, and thin. Therefore, we consider water as transparent liquid for visible wavelengths. Since water is transparent for visible light, the apparent spectral reflectance is the same as the original spectral reflectance in visible wavelengths independent of the presence/absence of water.

[†]We determine the scale of the apparent spectral reflectance so that its maximum value with respect to λ is 1 without loss of generality.

Then, we estimate the original spectral reflectance in NIR wavelengths from the apparent spectral reflectance in visible wavelengths. Specifically, on the basis of Eq. (1), we compute the coefficient c_n by solving the set of linear equations:

$$\hat{\rho}(\lambda_m) \approx \sum_{n=1}^N c_n b_n(\lambda_m), \quad (m = 1, 2, 3, \dots, M). \quad (3)$$

Here, λ_m is the visible wavelength at which the apparent spectral reflectance is given, and we set $M \geq N$. Substituting the computed coefficient c_n into Eq. (1), we obtain the original spectral reflectance $\rho(\lambda)$.

3.4 Per-Pixel Water Detection

Our proposed method detects water per pixel by exploiting the observation that the apparent spectral reflectance at a surface point is smaller than the original one in NIR wavelengths when water is present on the surface point. Specifically, we tested two measures. The first measure Q_1 is the sum of the difference between the estimated spectral reflectance $\rho(\lambda)$ and the apparent spectral reflectance $\hat{\rho}(\lambda)$ in NIR wavelengths $[\lambda_l, \lambda_h]$:

$$Q_1 = \sum_{\lambda=\lambda_l}^{\lambda_h} [\rho(\lambda) - \hat{\rho}(\lambda)]. \quad (4)$$

The second one Q_2 is the maximum value of the difference between the estimated spectral reflectance $\rho(\lambda)$ and the apparent spectral reflectance $\hat{\rho}(\lambda)$ in NIR wavelengths:

$$Q_2 = \max_{\lambda=[\lambda_l, \lambda_h]} [\rho(\lambda) - \hat{\rho}(\lambda)]. \quad (5)$$

Since $\rho(\lambda) \approx \hat{\rho}(\lambda)$ when water is absent, both the Q_1 and Q_2 take values near 0. On the other hand, since $\rho(\lambda) > \hat{\rho}(\lambda)$ when water is present, both the Q_1 and Q_2 take positive values. Thus, our method detect water by using thresholding Q_1 or Q_2 . In practice, due to the approximation errors in the low-dimensional linear model and the noises in hyperspectral images, both the Q_1 and Q_2 distribute around 0 and some positive values when water is absent and present respectively. Therefore, we evaluate the approximation errors of the spectral reflectances of the Munsell Color Book chips and some labeled samples, and then perform Receiver Operator Characteristic (ROC) analysis for determining the threshold [20]. In Sect. 4, we show that the measure based on the maximum difference Q_2 performs better than the straightforward measure Q_1 in terms of F-score.

4. Experiments

4.1 Low-Dimensional Linear Model Results

In this paper, the statistical structure of spectral reflectance is analyzed, and a low-dimensional linear combination model for the spectral reflectances from visible to NIR wavelengths is described. Similar to Parkkinen *et al.* [19], our analysis also based on the principal component analysis. We measured total of 1302 spectral reflectances from visible to NIR wavelengths from the Munsell Color Book chips with different hues, saturations, and values. In our proposed method, the first 10 principal components are used for reconstructing the measured spectral reflectance.

First, we obtained the basis vectors of the spectral reflectance from the visible to NIR wavelengths by using principal component analysis, and show the first five basis vectors in Fig. 3 (a). The first to fifth basis vectors are displayed in order of decreasing eigenvalues. The first eigenvector corresponds to the mean of the measured vectors, and its flatness indicates uniform covering of the color space. The cumulative contributions of eigenvalues are 0.9967 and 0.9997 for the first five and ten eigenvalues respectively.

In the second phase, we tested the reconstruction of the spectral reflectance by the basis vectors. In order to verify the feasibility of the linear approximation of the spectral reflectance from visible to NIR wavelengths, we have imported the real-world hyperspectral image dataset TokyoTech-dataset [21] (color images are shown in Fig. 3 (b)). The dataset contains 59-band hyperspectral images, including both visible and NIR spectral reflectance, of colorful objects with rich textures. Therefore, it is useful for the evaluation of various hyperspectral imaging and image restoration tasks. Figure 3 (c) represents some results of restoring the TokyoTech-dataset using our dataset. The dotted lines are the actual spectral reflectances and the solid lines are their approximations by using the low-dimensional linear model. We can see that the restoration results are very satisfactory; the RMSE error per band per pixel is 0.0183. It shows that the spectra reflectances of natural scenes can be reconstructed almost exactly by using 10 basis vectors.

4.2 Per-Pixel Water Detection Results

In the experiment, object surfaces were illuminated by a standard halogen lamp, and a hyperspectral camera manufactured by EBA JAPAN was used. We sampled spectral reflectances from 380 to 1000 nm at 5-nm intervals, and then obtained 125 bands of hyperspectral images. In this paper, we assume that object surfaces is illuminated by a light source of known spectral intensity. So, the spectral irradiance of the light source is measured by using a standard diffuse reflector. Then, the input spectral reflectances were obtained by dividing the spectral radiances by the measured spectral intensity of the light source. The process and results of the proposed method are shown in Fig. 4 (c-e).

First, we captured the hyperspectral images of scenes as with 125 bands. To facilitate understanding, we show the color images of the scenes by converting the hyperspectral images into the RGB images in Fig. 4(a).

Second, for each pixel, the apparent spectral reflectance in the visible wavelengths is used to estimate the original spectral reflectance in NIR wavelengths from 835 nm to 1000 nm (34bands). In this paper, we used 10 basis vectors, and the coefficients were computed from the apparent spectral reflectances between 380 nm to 830 nm (91bands).The apparent and estimated spectral reflectances at surface points without and with water are shown in Fig. 4 (c) and (d) respectively. Here, the solid red and blue lines are for the apparent spectral reflectances, and the black dotted lines are for the estimated original spectral reflectances. As shown in Fig. 4(c)(d), water is transparent for visible wavelengths, and then the appearance of water on an object surface significantly depends not on the water itself but on the background object surface. The apparent spectral reflectance and original spectral reflectance are almost the same for visible wavelengths. On the other hand, in NIR wavelengths, the brightness of an object surface on which water is present is smaller than that without water, because NIR light, incoming to and outgoing from the object surface, is absorbed by water. In other words, the apparent spectral reflectance is smaller when water is present. In NIR wavelengths, as shown in Fig. 4(c), the apparent spectral reflectance without water is almost the same as the estimated original spectral reflectance. However, as shown in Fig. 4 (d), the apparent spectral reflectance is smaller than the estimated original spectral reflectance.

Finally, (e) the histogram of the difference measure Q_1 or Q_2 over the entire image is made on the basis of Eq. (3). The optimal threshold for classifying surface points with/without water is determined by ROC analysis with some samples with the ground truth labels. We used the threshold to perform binary classification on a test scene.

4.3 Comparison with Existing Methods

We tested the performance of water detection on unknown and complex backgrounds using complex textured cloths

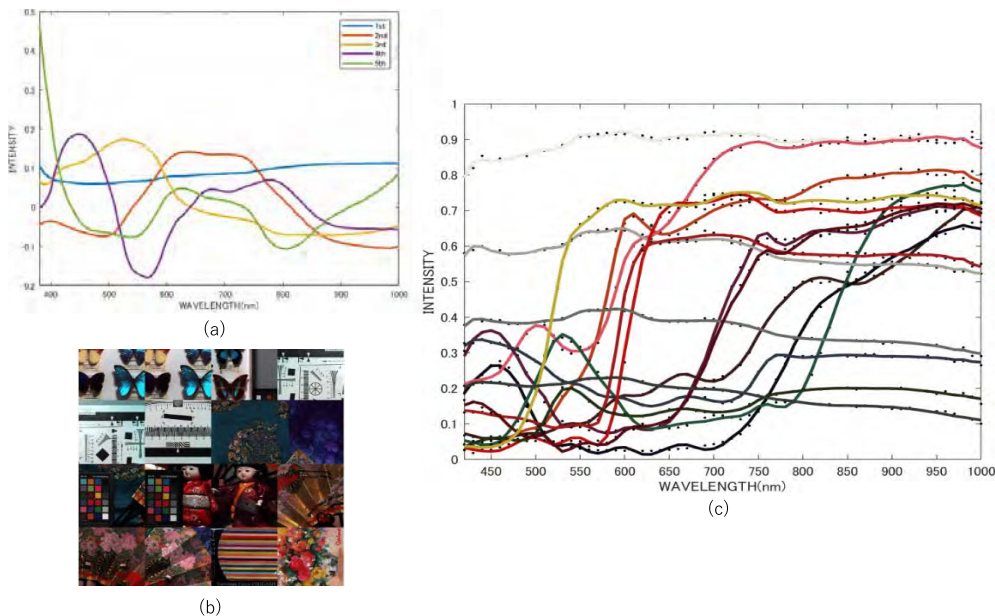


Fig. 3 (a) Basis vector of spectral reflectances from visible to near-infrared. The first to fifth basis vector are displayed in order of decreasing eigenvalues. (b) TokyoTech-dataset samples in color images. (c) Restoration results (using our dataset for TokyoTech-dataset [21]). The RMSE per band per pixel is 0.0183.

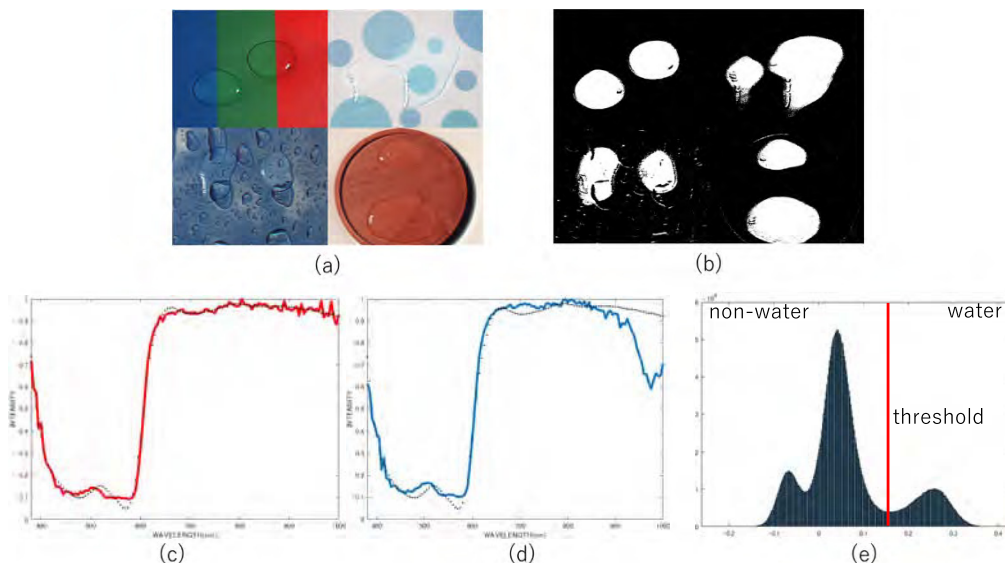


Fig. 4 The process and results of the method: (a) the color images of the targets converted from the hyperspectral images, (b) the results of water detection; white/black stand for with/without water, (c) the apparent spectral reflectance of a pixel in the image without water (solid red line), (d) the apparent spectral reflectance of a pixel in the image with water (solid blue lines). The dotted black lines in (c) and (d) are the estimated original spectral reflectances, (e) the histogram of the difference between the estimated spectral reflectance and the apparent spectral reflectance.

((1)-(4)) and 6 different colors of leather ((5)-(6)) as objects. Odd numbers are non-water scenes and even numbers are water scenes. In order to obtain the ground truth labels for quantitative analysis, we first captured the image of the surface without water, and then captured the image of the object surface with water, and made positive solution labels by finding differences and active contour [22].

To confirm the effectiveness of our proposed method, we compared the performance of our method with those of

the following methods.

NIR975nm (method based on only one NIR band) : In the wavelengths of 380 to 1000 nm, we selected the wavelength of 975 nm at which the water absorption is maximum, and then used the apparent spectral reflectance at that band as input.

NIROnly (method based on ratio of the short-wave infrared bands) [10] : We used the ration of apparent spectral reflectances at two different wavelengths in

NIR, 975 nm/830 nm, at which water absorption is maximum/minimum.

DTDCA (method based on orthogonal subspace projection) [17] : The relative water absorption is given as the detection target, the background is estimated, and the score of the detector is used as an input. This is a common method, please refer to [17] for detail.

WI2015 (method based on linear discriminant analysis) [11] : We assume the water absorption is known. The same statistical analysis was used to determine the coefficients that best separated the training class, like those which minimize the within-class variance and maximize the between-class variance, using linear discriminant analysis classification. The training pixels included images with water and without water. Then, we obtain the feature vector and use the normalized value of the linear combination of the recognition object and the feature vector as input. In particular, we use visible to NIR wavelengths instead of visible to shortwave infrared wavelengths (in the existing method) as objects.

NDWI [23] and HDWI [24] : NDWI and HDWI are well-known indices for water detection. Since the spectral range of our hyperspectral camera is limited from 380 nm to 1000 nm, we define NDWI as $NDWI = (Green - NIR)/(Green + NIR)$, where the Green and NIR bands are [490,580]nm and [780,860]nm respectively. We define HDWI as $HDWI = (Red - NIR)/(Red + NIR)$, where the Red and NIR bands are [650,700]nm and [705,850]nm respectively.

RXD (method based on Reed-XiaoLi detector) [25] : Algorithms commonly used in spectral anomaly detection, please refer to [25] for details.

VSM (method based on vector-subspace model) [26] : The VSM method also makes use of the low-dimensional linear model in a similar manner to ours, but the way of calculating the coefficients is different. The VSM method uses the reflectance from visible to NIR wavelengths instead of NIR wavelength in Eq. (3).

We compared the performance of our proposed method with those of closely related methods. The performances were evaluated by using the receiver operator characteristic (ROC) curves, which plot the true positive rate (TPR) against the false positive rate (FPR) for a range of threshold values [20]. TPR is the percentage of reference water pixels that are correctly classified, and FPR is the percentage of reference non-water pixels incorrectly classified as water.

Different methods have different shaped ROC curves, reflecting their variable accuracies in classifying the data across different thresholds (Fig. 5). Ours are the steepest (closer to the top left in Fig. 5), representing more accurate results than the other indexes across a limited range of thresholds. Across the full range of thresholds, Ours achieves the highest area under the ROC curve (see AUC in Table 1), as the index is more accurate when conservative or liberal thresholds are used.

In addition, we also introduced recall, precision, and F-score for quantitative analysis. The results are shown

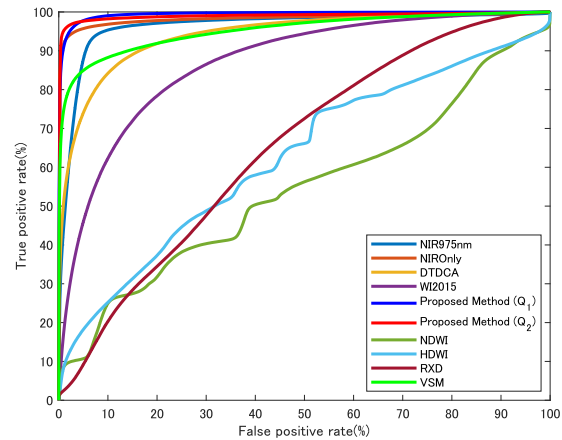


Fig. 5 The ROC curves for our proposed method and the existing methods.

Table 1 The quantitative comparison with the closely related existing methods in terms of Recall, Precision, F-score, and AUC.

Method	Recall	Precision	F-score	AUC
Ours (Q_2)	0.9196	0.9065	0.9130	0.9896
Ours (Q_1)	0.8559	0.8934	0.8742	0.9939
NIR975nm	0.7447	0.5053	0.6021	0.9635
NIROnly [10]	0.8699	0.9190	0.8938	0.9828
DTDCA [17]	0.5593	0.6315	0.5932	0.9409
WI2015 [11]	0.4287	0.3034	0.3553	0.8689
HDWI [24]	0.2511	0.0989	0.1419	0.5439
NDWI [23]	0.1601	0.1576	0.1588	0.6261
RXD [25]	0.2635	0.0790	0.1215	0.6513
VSM [26]	0.7119	0.8268	0.7651	0.9521

in Table 1. First, due to the influence of the near-infrared light absorption of water and the reflectance of the surface itself, the NIR method (NIR975nm) using only one band has a higher recall, but the precision is extremely low. A method that takes account of the changes in the absorption rate (NIROnly) reduces the recall rate and improves precision. This is because the difference in reflectance of the background itself is not taken into account. This is why the AUC and F-score of both methods are not so high. Second, in the method of simply estimating the reflectance of the surface of the object (DTDCA), it can be seen that compared with the above methods, the AUC is improved, but the F-score is low. This is because the transparent color of water in the visible range shows the background color, which results in large errors for backgrounds. Third, in the method of classifying water background and anhydrous background with LDA (WI2015), the results of water thickness and noise cannot be considered, so the method does not work well. Fourth, Table 1 clearly shows that NDWI, HDWI, and RXD methods are not suitable for detecting water on the surface with spatially-varying reflectance. Fifth, VSM method is not as good as our method. Because the VSM method uses the reflectance from visible to NIR wavelengths, and then the coefficients are contaminated by the apparent reflectance at NIR wavelengths when water is present. This is a possible reason for false negatives (Fig. 6 (1)-(6)). Finally, considering the relationship between visible light, NIR, and the spectral characteristics of water, the recall, and precision of our

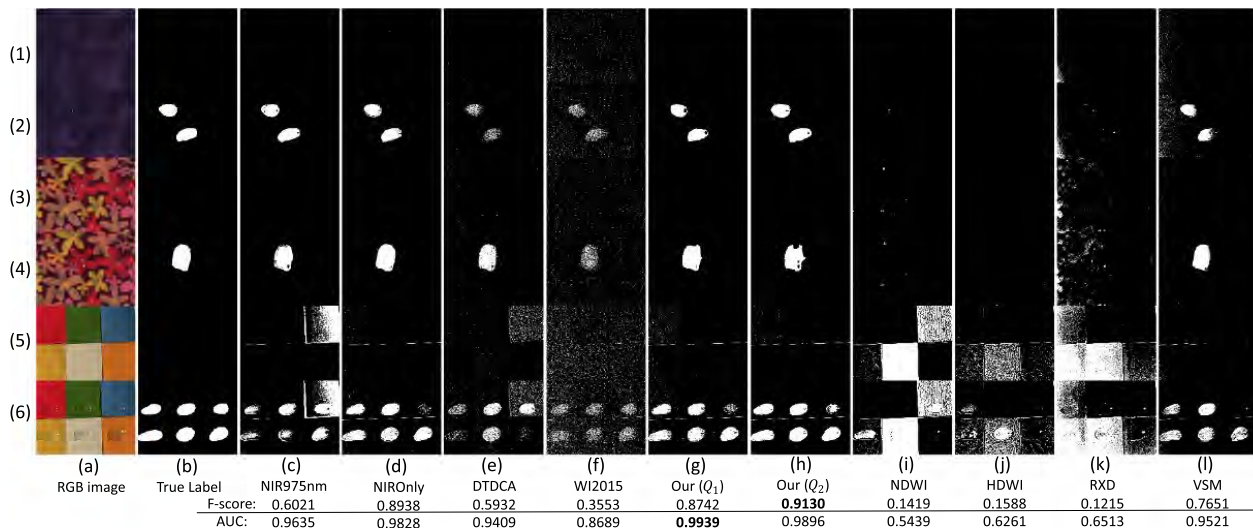


Fig. 6 The experimental results : (a) The scene is shown in the RGB image (water is absent/present in the scenes with odd/even numbers), (b) true labels, and the result images of methods: (c) NIR975nm, (d) NIROnly method, (e) DTDCa, (f) WI2015, (g) ours with Q_1 , (h) ours with Q_2 , (i) NDWI, (j) HDWI, (k) RXD, and (l) VSM.

method is a good balance. Our method also has a higher F-score and AUC than existing methods. At the same time, we can also see that our method (Q_2) is better than our method (Q_1) in terms of F-score. This may be caused by the additive noises in the captured hyperspectral images, and the approximation errors of the low-dimensional linear model.

In Fig. 6, we show (c-d) a method using only NIR, (e) the existing method based on background estimation, and (f) the existing method based on LDA classification. First, Fig. 6 (c) shows that the NIR single-band method is difficult to classify the originally small reflectance in near-infrared and the small reflectance due to water absorption. This is the reason why some colors are detected as water. We can see that in Fig. 6 (d), the results of using only NIR have false negative. We can see that part of the water is considered to be background (as shown in Fig. 6 (d)-(6)). This is caused by the surface with spatially-varying reflectance. Our method has false negative too due to specular reflection on the water surface. Ours may be solved by using a polarizing filter. Second, in Fig. 6 (e), it can be seen that the overall detection result is not clearer than the NIR only method due to using background estimating. Unfortunately, because water is transparent for visible light, resulting in water with multiple visible range reflectances. This is why relying solely on the NIR absorption of water as a target may result in incorrect estimates of the reflectance of background components. Third, as shown in Fig. 6 (f), the results are not well due to errors caused by different water depths and noise. Finally, Fig. 6 (h) clearly shows that our method (Q_2) performs better than the above methods. At the same time, in Fig. 6 (g), we can also see that our method (Q_1) detects water when there is no water in the background. There are two reasons for errors. The first reason is noises in the hyperspectral images. The second reason is the use of the low-dimensional linear model; its approximation accuracy is limited when a small number of basis functions is used.

5. Conclusion and Future Work

In this paper, we proposed a method for per-pixel water detection on surfaces with unknown and spatially-varying reflectance. Our proposed method estimates the original spectral reflectance at each surface point in NIR wavelengths from its apparent spectral reflectance in visible wavelengths. Specifically, we make use of the low-dimensional linear combination model for spectral reflectance from visible to NIR wavelengths. Then, water is detected on the basis of the difference between the estimated original spectral reflectance and the apparent one in NIR wavelengths. We conducted a number of experiments using real images, and confirmed that our proposed method performs better than the existing technology. In the future, we will reduce the number of bands to design a simple camera for water detection.

Acknowledgments

This work was supported by JSPS KAKENHI Grant Numbers JP17H01766 and JP20H00612.

References

- [1] A. Khelloufi, N. Achour, R. Passama, and A. Cherubini, "Tentacle-based moving obstacle avoidance for omnidirectional robots with visibility constraints," 2017 IEEE/RSJ Int. Conf. Intelligent Robots and Systems (IROS), pp.1331–1336, IEEE, 2017.
- [2] B. Ichter, J. Harrison, and M. Pavone, "Learning sampling distributions for robot motion planning," 2018 IEEE Int. Conf. Robot. Autom. (ICRA), pp.7087–7094, IEEE, 2018.
- [3] F. Pernkopf and P. O'Leary, "Image acquisition techniques for automatic visual inspection of metallic surfaces," NDT & E International, vol.36, no.8, pp.609–617, Dec. 2003.
- [4] S. Agnisarman, S. Lopes, K.C. Madathil, K. Piratla, and A. Gramopadhye, "A survey of automation-enabled human-in-the-loop

- systems for infrastructure visual inspection,” *Automation in Construction*, vol.97, pp.52–76, Jan. 2019.
- [5] J.A. Curcio and C.C. Petty, “The near infrared absorption spectrum of liquid water,” *JOSA A*, vol.41, no.5, pp.302–304, 1951.
- [6] Y. Zhou, J. Dong, X. Xiao, T. Xiao, Z. Yang, G. Zhao, Z. Zou, and Y. Qin, “Open surface water mapping algorithms: A comparison of water-related spectral indices and sensors,” *Water*, vol.9, no.4, p.256, 2017.
- [7] T. Bijeesh and K. Narasimhamurthy, “Surface water detection and delineation using remote sensing images: A review of methods and algorithms,” *Sustainable Water Resources Management*, vol.6, no.4, pp.1–23, 2020.
- [8] A. Rankin and L. Matthies, “Daytime water detection based on color variation,” 2010 IEEE/RSJ Int. Conf. Intelligent Robots and Systems, pp.215–221, IEEE, 2010.
- [9] A.L. Rankin, L.H. Matthies, and P. Bellutta, “Daytime water detection based on sky reflections,” 2011 IEEE Int. Conf. Robot. Autom., pp.5329–5336, IEEE, 2011.
- [10] M. Bertozzi, R.I. Fedriga, and C. D’Ambrosio, “Adverse driving conditions alert: investigations on the swir bandwidth for road status monitoring,” *Int. Conf. Image Analysis and Processing*, pp.592–601, Springer, 2013.
- [11] A. Fisher, N. Flood, and T. Danaher, “Comparing landsat water index methods for automated water classification in eastern australia,” *Remote Sensing of Environment*, vol.175, pp.167–182, March 2016.
- [12] M. Shimano, H. Okawa, Y. Asano, R. Bise, K. Nishino, and I. Sato, “Wetness and color from a single multispectral image,” *Proc. IEEE Conf. Comput. Vis. Pattern Recognit.*, pp.3967–3975, 2017.
- [13] H. Okawa, M. Shimano, Y. Asano, R. Bise, K. Nishino, and I. Sato, “Estimation of wetness and color from a single multispectral image,” *IEEE Trans. Pattern Anal. Mach. Intell.*, 2019.
- [14] Y. Asano, Y. Zheng, K. Nishino, and I. Sato, “Shape from water: Bispectral light absorption for depth recovery,” *European Conf. Comput. Vis.*, pp.635–649, Springer, 2016.
- [15] J.M. Bioucas-Dias, A. Plaza, G. Camps-Valls, P. Scheunders, N. Nasrabadi, and J. Chanussot, “Hyperspectral remote sensing data analysis and future challenges,” *IEEE Geoscience and remote sensing magazine*, vol.1, no.2, pp.6–36, June 2013.
- [16] C.I. Chang, Q. Du, T.L. Sun, and M.L. Althouse, “A joint band prioritization and band-decorrelation approach to band selection for hyperspectral image classification,” *IEEE Trans. geoscience and remote sensing*, vol.37, no.6, pp.2631–2641, Nov. 1999.
- [17] H. Ren and C.I. Chang, “Automatic spectral target recognition in hyperspectral imagery,” *IEEE Trans. Aerospace and Electronic Systems*, vol.39, no.4, pp.1232–1249, Oct. 2003.
- [18] A. Chakrabarti and T. Zickler, “Statistics of real-world hyperspectral images,” *CVPR 2011*, pp.193–200, IEEE, 2011.
- [19] J.P.S. Parkkinen, J. Hallikainen, and T. Jaaskelainen, “Characteristic spectra of munsell colors,” *JOSA A*, vol.6, no.2, pp.318–322, 1989.
- [20] T. Fawcett, “An introduction to roc analysis,” *Pattern Recognit. Lett.*, vol.27, no.8, pp.861–874, June 2006.
- [21] Y. Monno, H. Teranaka, K. Yoshizaki, M. Tanaka, and M. Okutomi, “Single-sensor rgb-nir imaging: High-quality system design and prototype implementation,” *IEEE Sensors Journal*, vol.19, no.2, pp.497–507, 2018.
- [22] T.F. Chan and L.A. Vese, “Active contours without edges,” *IEEE Trans. Image Process.*, vol.10, no.2, pp.266–277, Feb. 2001.
- [23] S.K. McFeeters, “The use of the normalized difference water index (ndwi) in the delineation of open water features,” *International journal of remote sensing*, vol.17, no.7, pp.1425–1432, 1996.
- [24] H. Xie, X. Luo, X. Xu, X. Tong, Y. Jin, H. Pan, and B. Zhou, “New hyperspectral difference water index for the extraction of urban water bodies by the use of airborne hyperspectral images,” *J. Applied Remote Sensing*, vol.8, no.1, p.085098, 2014.
- [25] I.S. Reed and X. Yu, “Adaptive multiple-band cfar detection of an optical pattern with unknown spectral distribution,” *IEEE Trans. Acoust., Speech, Signal Process.*, vol.38, no.10, pp.1760–1770, Oct.

1990.

- [26] T. Jaaskelainen, J. Parkkinen, and S. Toyooka, “Vector-subspace model for color representation,” *JOSA A*, vol.7, no.4, pp.725–730, 1990.



Chao Wang received his B.S. in Computer Science and Technology from Shenyang University of Technology in 2015. Also, he received an M.S. in Advanced Information Engineering from Kyushu Institute of Technology in 2018. Currently, he is studying for a Ph.D. in Information Engineering from Kyushu Institute of Technology. His research includes computer vision and machine learning. He holds keen interests in the area of hyperspectral imaging, and material classification.



Michihiko Okuyama received his B.S. in Intelligent Information Engineering from Kyushu Institute of Technology in 2019. He holds keen interests in the area of computer vision, and image processing.



Ryo Matsuoka received the B.E., M.E., and Ph.D. degrees from The University of Kitakyushu, Kitakyushu, Japan, in 2011, 2013, and 2016, respectively. He has been an Assistant Professor in the Faculty of Engineering, Kagawa University from 2016 to 2018. In 2019, he has also been an Assistant Professor in the Department of Artificial Intelligence, Kyushu Institute of Technology. He is currently with the Faculty of Environmental Engineering, The University of Kitakyushu, as an Associate Professor. His research interests are in image processing and computer vision. He received the Excellent Award of the Hibikino Award for master’s thesis and the Excellent Student Award of the IEEE Fukuoka Section in 2013.



Takahiro Okabe Takahiro Okabe received his B.S. and M.S. degrees in physics, and his Ph.D. degree in information science and technology from the University of Tokyo, Japan, in 1997, 1999, and 2011 respectively. After working at Institute of Industrial Science, the University of Tokyo, he joined Kyushu Institute of Technology, Japan, as an associate professor in 2013. He is currently with Department of Artificial Intelligence, Kyushu Institute of Technology, as a professor. He was a visiting scholar at Tübingen University, Germany, from 2011 to 2012. His research interests include computer vision, computational photography, image processing, pattern recognition, and computer graphics, in particular their physical and mathematical aspects. He received the IEICE Best Paper Awards in 2006, 2008, and 2010.